Effects of viscosity and acoustic streaming on the interparticle radiation force between rigid spheres in a standing wave

Shahrokh Sepehrirahnama,* Fook Siong Chau,† and Kian-Meng Lim‡
Department of Mechanical Engineering, National University of Singapore, Singapore 117575, Singapore
(Received 22 August 2015; revised manuscript received 19 December 2015; published 26 February 2016)

The total acoustic radiation force acting on interacting spheres in a viscous fluid consists of the primary and secondary forces. The primary force pushes rigid spheres to the pressure node due to the incident standing wave. The secondary force is the interparticle force caused by the interaction between spheres in the standing wave. In this study, an algorithm based on the multipole series expansion and Stokeslet method is proposed for calculating the primary and secondary radiation forces acting on a pair of spheres in a viscous fluid. It is concluded that the acoustical interaction between a pair of spheres is considerably stronger in a viscous fluid compared to the inviscid case due to the streaming effects in the viscous fluid. For spheres located far from each other, the interaction becomes considerably weak; thus, the spheres move mainly due to the primary radiation force.

DOI: 10.1103/PhysRevE.93.023307

I. INTRODUCTION

Manipulation of particles in microchannels using ultrasound waves, commonly known as acoustophoresis, has attracted a lot of attention in the past decade. Generally, in the sound field, particles start moving under the primary acoustic radiation force towards either the pressure node or antinode depending on their acoustic contrast factor. When particles stay long enough in the sound field, especially when the fluid is stationary, agglomeration occurs, mainly due to the interaction among the particles, i.e., repulsion or attraction. Hence, taking the secondary (interparticle) radiation force into account will result in future enhancements of the particle manipulation. Nevertheless, experimental measurement techniques and methods for theoretical calculations of the secondary force are difficult and not well established as compared to the primary force.

In the literature, the acoustical interaction between particles has been studied extensively for inviscid fluid [1–12]. Early studies discussed the calculation of the Bjerknes force, which is fundamentally equivalent to the acoustic interparticle force, based on the idea of rescattering of the scattered waves from each particle [1–7,9,11,12]. It is noted that only an approximate solution is given by the rescattering approach since the rescattering of the waves, which occurs infinitely, is truncated to a finite number of times during the calculation [8,10]. Most of the formulations derived by this approach are accurate up to the second order [1–7,9,11–17].

The other approach to obtain scattered waves from particles is to solve the scattering problem for all the particles simultaneously [8,10]. Generally, this approach requires a numerical computation since the system of equations derived from the boundary conditions is fully coupled, especially when the particles are close to each other. After obtaining the scattered waves, one can calculate the interparticle force by integrating the corresponding stresses on the surface of each particle. This approach is more accurate compared to the rescattering approach since it guarantees the boundary conditions imposed on all the particles simultaneously. More details of this approach can be found in Refs. [8,10].

The addition of fluid viscosity to the acoustic interaction has two implications. First, the viscous loss affects the scattered pressure waves and also generates shear waves [18–20]. Second, the acoustic streaming is triggered by the viscosity and it causes additional viscous tractions on the surface of the particles [21,22]. By solving the acoustic streaming equations for the case of multiple particles, one can calculate the additional drag on each particle induced by the presence of other particles. For the case of particles in an infinite domain, the Rayleigh streaming and its counterpart, Schlichting streaming, are generated around each individual particle by the scattered waves. It has been shown that the effect of Eckart streaming is small and negligible for the case of a plane standing wave [22]. It is also noted that the streaming from the particles should be considered in a coupled manner, similar to the calculation of the scattered waves, to avoid any loss in the accuracy of the results.

In the context of pulsating bubble dynamics, the acoustical interaction force has been studied both theoretically and experimentally. However, theoretical studies are limited to simple cases for the calculation of the secondary force on small bubbles in the Rayleigh limit ($ka \ll 1$). Only radial and translational velocities of the bubble surface which are equivalent to monopole and dipole shape oscillations were considered. The latest study by Doinikov [2] included the first-order effects of the viscosity and the acoustic streaming solution for the case of pulsating bubbles which are far apart from each other so as to neglect higher-order spherical harmonics. More details on the secondary Bjerknes force acting on pulsating bubbles can be found in Refs. [1–7].

Here, we propose a numerical algorithm for calculation of the primary and total radiation force acting on rigid spheres with the inclusion of the viscosity and acoustic streaming effects. The primary objective is to study and quantify the impact of viscosity on the acoustical interaction between rigid spheres in a sound field. First, the primary radiation force is estimated by the far-field series solution, proposed by Balachandar *et al.* [19]. Then, in order to include the viscosity and acoustic streaming, the total radiation force is calculated

*shahrokh.sepehri@u.nus.edu
†mpecfs@nus.edu.sg
‡limkm@nus.edu.sg

by using the multipole series expansion and Stokeslet method. Ultimately, the secondary (interparticle) radiation force is approximated as the difference between the total and primary radiation forces. This numerical algorithm has no restriction on the size of the spheres because of the use of higher-order multipole terms. It is applicable to all separation distances and only breaks down when the spherical particles are in contact with each other. Although the methodology is demonstrated for rigid spheres, it is easily extended to compressible spheres by including the pressure field in the spheres.

II. METHODOLOGY

The acoustical interaction problem is usually formulated for a pair of spheres [2,8–10], as shown in Fig. 1. A local spherical coordinate is attached to each sphere. For stationary viscous fluid, the primary and secondary radiation forces, along with the viscous drag, are exerted on each sphere in the sound field. For a plane standing wave, it has been shown that the drag force generated from the acoustic streaming induced by the incident wave is negligible [21,22]. Hence, the total force is the sum of the primary and secondary (interparticle) radiation forces.

According to the perturbation theory, the fluid velocity $\mathbf{v}$, pressure p, and density ρ with accuracy up to the second order are expressed as

$$\begin{aligned} \mathbf{v} &= \mathbf{v}_1 + \mathbf{v}_2, \\ p &= p_0 + p_1 + p_2, \\ \rho &= \rho_0 + \rho_1 + \rho_2, \end{aligned} \tag{1}$$

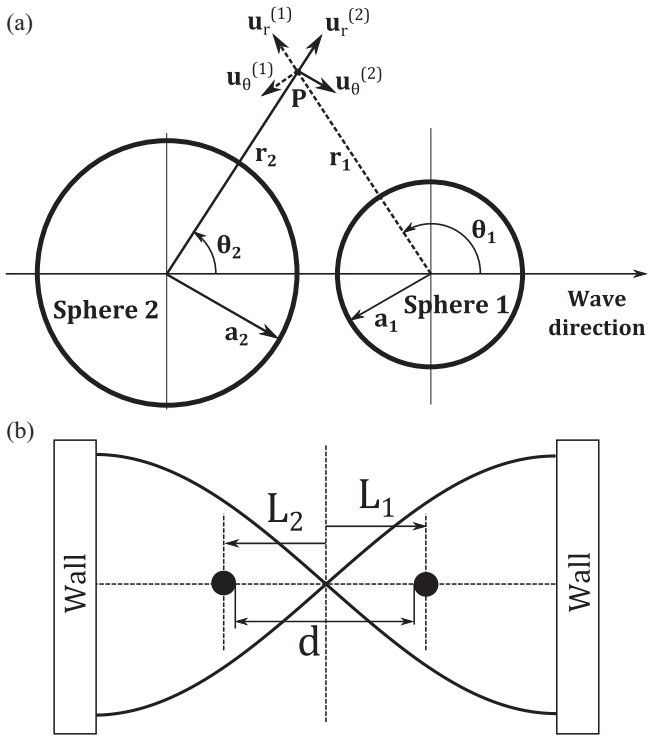

FIG. 1. (a) A pair of spherical particles in an axisymmetric configuration with their local spherical coordinate systems. (b) The distance between the particles is denoted by d and their positions with respect to the pressure nodal line are denoted by L_1 and L_2.

where the indices 0, 1, and 2 show the zeroth-, first-, and second-order variables, respectively. The fluid is assumed to be stationary; thus, the zero-order velocity is zero. The first-order time-harmonic velocity, pressure, and density, governed by the the acoustic wave equation in a viscous fluid, are written in terms of scalar and vector potentials as follows [19,22]:

$$\begin{aligned} \mathbf{v}_1 &= \nabla\phi + \nabla \times \Psi, \\ p_1 &= i\rho_0\omega\phi, \\ \rho_1 &= i\frac{\omega}{c^2}\rho_0\phi, \end{aligned} \tag{2}$$

where c is the speed of sound in the host fluid, ω is the angular frequency, i is the complex variable, and ϕ and Ψ are the first-order scalar and vector potentials, respectively. For a pair of spheres, the scalar and vector potentials are obtained as

$$\phi = \phi_i + \phi_s^{(1)} + \phi_s^{(2)}, \quad \Psi = \Psi_s^{(1)} + \Psi_s^{(2)}, \tag{3}$$

where ϕ_i is the scalar potential of the incident wave, and $\phi_s^{(j)}$ and $\Psi_s^{(j)}$ are the scalar and vector potentials of the scattered wave from the jth sphere ($j = 1$ or 2), respectively. The scalar potential of the incident wave ϕ_i can be expanded using a multipole series as [23,24]

$$\phi_i = e^{-i\omega t}\sum_{n=0}^{\infty} A_n j_n(k_c r) P_n(\nu), \tag{4}$$

where k_c is the compression wave number, $j_n(k_c r)$ is the spherical Bessel function of order n, $P_n(\nu)$ is the Legendre polynomial of order n and $\nu = \cos(\theta)$, A_n is the multipole coefficient, and r and θ are the global spherical coordinates located at the pressure node. The compression wave number is given as [19,25]

$$k_c = k\left[1 - \frac{ik}{\rho_0 c}\left(\xi + \frac{4}{3}\mu\right)\right]^{-1/2}, \tag{5}$$

where $k = 2\pi/\lambda$ is the nominal wave number and λ is the wavelength of the acoustic wave in the fluid medium, and ξ and μ are the bulk and dynamic viscosity of the host fluid, respectively. For a plane standing wave, the multipole coefficients of the incident wave series expansion are given as

$$\begin{aligned} A_n^{(1)} &= \frac{\Phi_0}{2} i^n (2n+1)[e^{ikL_1} + (-1)^n e^{ikL_1}], \\ A_n^{(2)} &= \frac{\Phi_0}{2} i^n (2n+1)[e^{ikL_2} + (-1)^n e^{ikL_2}], \end{aligned} \tag{6}$$

where $A_n^{(1)}$ and $A_n^{(2)}$ are the coefficients of the series expanded about the local spherical coordinates attached to sphere 1 and sphere 2, respectively; Φ_0 is the amplitude of the incident wave and L_1 and L_2 are the positions of sphere 1 and 2, respectively, measured from the pressure node, as shown in Fig. 1. For the jth sphere, the multipole series expansions of the scalar and vector potentials of the scattered wave are expressed as [19,22]

$$\begin{aligned} \phi_s^{(j)} &= e^{-i\omega t}\sum_{n=0}^{\infty} B_n^{(j)} h_n(k_c r_j) P_n(\nu_j), \\ \Psi_s^{(j)} &= \mathbf{u}_\varphi^{(j)} e^{-i\omega t}\sum_{n=0}^{\infty} C_n^{(j)} h_n(k_s r_j)\frac{dP_n(\nu_j)}{d\theta_j}, \end{aligned} \tag{7}$$

where k_s is the shear wave number, ν_j is equal to $\cos(\theta_j)$, r_j and θ_j are the local spherical coordinates with respect to the jth sphere, $h_n(\bullet)$ is the Hankel function of the first kind and order n, $\mathbf{u}_\varphi^{(j)}$ is the local unit vector in the azimuthal angle direction, and $B_n^{(j)}$ and $C_n^{(j)}$ are the multipole coefficients of the scalar and vector potentials of the scattered wave from the jth sphere, respectively. The shear wave number is $k_s = (1+i)/\delta$, where $\delta = \sqrt{2\mu/(\rho_0\omega)}$ is the viscous penetration depth [22,25]. To obtain the multipole coefficients $B_n^{(j)}$ and $C_n^{(j)}$, the first-order boundary conditions are imposed by the weighted residue technique as follows:

$$\int_{S^{(j)}} P_n(\nu_j)\left(\mathbf{v}_1 \cdot \mathbf{u}_r^{(j)}\right) dS = 0,$$
$$\int_{S^{(j)}} \frac{dP_n(\nu_j)}{d\theta_j}\left(\mathbf{v}_1 \cdot \mathbf{u}_\theta^{(j)}\right) dS = 0, \tag{8}$$

where $dS = 2\pi a_j \sin\theta_j d\theta_j$ and a_j is the radius of the jth sphere, and $\mathbf{u}_r^{(j)}$ and $\mathbf{u}_\theta^{(j)}$ are the radial and tangential basis vectors of the local spherical coordinate attached to the jth sphere, as shown in Fig. 1. The Legendre polynomials and their first derivatives are chosen to be the weights because of their orthogonal property. For a pair of spheres, the final set of equations, after assembling the matrices, is written as

$$\begin{bmatrix} \mathbf{K}^{(11)} & \mathbf{K}^{(12)} \\ \mathbf{K}^{(21)} & \mathbf{K}^{(22)} \end{bmatrix} \begin{Bmatrix} \mathbf{B}^{(1)} \\ \mathbf{C}^{(1)} \\ \mathbf{B}^{(2)} \\ \mathbf{C}^{(2)} \end{Bmatrix} = \begin{bmatrix} \mathbf{S}^{(1)} \\ \mathbf{S}^{(2)} \end{bmatrix} \begin{Bmatrix} \mathbf{A}^{(1)} \\ \mathbf{A}^{(2)} \end{Bmatrix}, \tag{9}$$

where $\mathbf{A}^{(j)}$ are the multipole coefficients of the incident wave obtained by substituting the position of the jth sphere, L_j, into Eq. (6). For numerical calculations, only the terms up to order M are included in the multipole series expansions. The size of the square submatrix $\mathbf{K}$ and subvector $\mathbf{S}$ is $2M+1$. The size of subvector B is $M+1$ whereas C is the subvector of size M since the vector potential has no monopole term. For two spheres, the elements of the submatrices $\mathbf{K}$ and $\mathbf{S}$ are expressed as follows:

$$\begin{aligned}
\mathbf{K}^{(11)}: K_{(l+1)(q+1)} &= -\int_{S_1} P_l(\nu_1)\frac{d}{dr_1}[h_q(k_c r_1)P_q(\nu_1)]dS_1, \\
K_{(l+1)(q+M+1)} &= -\int_{S_1} \frac{P_l(\nu_1)}{r_1\sin\theta_1}\frac{d}{d\theta_1}\left[\sin\theta_1 h_q(k_s r_1)\frac{dP_q(\nu_1)}{d\theta_1}\right]dS_1, \quad q \neq 0, \\
K_{(l+M+1)(q+1)} &= -\int_{S_1} \frac{dP_l(\nu_1)}{d\theta_1}\frac{1}{r_1}\frac{d}{d\theta_1}[h_q(k_c r_1)P_q(\nu_1)]dS_1, \quad n \neq 0, \\
K_{(l+M+1)(q+M+1)} &= \int_{S_1} \frac{dP_l(\nu_1)}{d\theta_1}\frac{1}{r_1}\frac{d}{dr_1}\left[r_1 h_q(k_s r_1)\frac{dP_q(\nu_1)}{d\theta_1}\right]dS_1, \quad n,q \neq 0;
\end{aligned} \tag{10}$$

$$\begin{aligned}
\mathbf{K}^{(12)}: K_{(l+1)(q+1)} &= -\int_{S_1} P_l(\nu_1)\frac{d}{dr_1}[h_q(k_c r_2)P_q(\nu_2)]dS_1, \\
K_{(l+1)(q+M+1)} &= -\int_{S_1} \frac{P_l(\nu_1)}{r_1\sin\theta_1}\frac{d}{d\theta_1}\left[\sin\theta_1 h_q(k_s r_2)\frac{dP_q(\nu_2)}{d\theta_2}\right]dS_1, \quad q \neq 0, \\
K_{(l+M+1)(q+1)} &= -\int_{S_1} \frac{dP_l(\nu_1)}{d\theta_1}\frac{1}{r_1}\frac{d}{d\theta_1}[h_q(k_c r_2)P_q(\nu_2)]dS_1, \quad n \neq 0, \\
K_{(l+M+1)(q+M+1)} &= \int_{S_1} \frac{dP_l(\nu_1)}{d\theta_1}\frac{1}{r_1}\frac{d}{dr_1}\left[r_1 h_q(k_s r_2)\frac{dP_q(\nu_2)}{d\theta_2}\right]dS_1, \quad n,q \neq 0;
\end{aligned} \tag{11}$$

$$\begin{aligned}
\mathbf{K}^{(21)}: K_{(l+1)(q+1)} &= -\int_{S_2} P_l(\nu_2)\frac{d}{dr_2}[h_q(k_c r_1)P_q(\nu_1)]dS_2, \\
K_{(l+1)(q+M+1)} &= -\int_{S_2} \frac{P_l(\nu_2)}{r_2\sin\theta_2}\frac{d}{d\theta_2}\left[\sin\theta_2 h_q(k_s r_1)\frac{dP_q(\nu_1)}{d\theta_1}\right]dS_2, \quad q \neq 0, \\
K_{(l+M+1)(q+1)} &= -\int_{S_2} \frac{dP_l(\nu_2)}{d\theta_2}\frac{1}{r_2}\frac{d}{d\theta_2}[h_q(k_c r_1)P_q(\nu_1)]dS_2, \quad n \neq 0, \\
K_{(l+M+1)(q+M+1)} &= \int_{S_2} \frac{dP_l(\nu_2)}{d\theta_2}\frac{1}{r_2}\frac{d}{dr_2}\left[r_2 h_q(k_s r_1)\frac{dP_q(\nu_1)}{d\theta_1}\right]dS_2, \quad n,q \neq 0;
\end{aligned} \tag{12}$$

$$\begin{aligned}
\mathbf{K}^{(22)}: K_{(l+1)(q+1)} &= -\int_{S_2} P_l(\nu_2)\frac{d}{dr_2}[h_q(k_c r_2)P_q(\nu_2)]dS_2, \\
K_{(l+1)(q+M+1)} &= -\int_{S_2} \frac{P_l(\nu_2)}{r_2\sin\theta_2}\frac{d}{d\theta_2}\left[\sin\theta_2 h_q(k_s r_2)\frac{dP_q(\nu_2)}{d\theta_2}\right]dS_2, \quad q \neq 0, \\
K_{(l+M+1)(q+1)} &= -\int_{S_2} \frac{dP_l(\nu_2)}{d\theta_2}\frac{1}{r_2}\frac{d}{d\theta_2}[h_q(k_c r_2)P_q(\nu_2)]dS_2, \quad n \neq 0, \\
K_{(l+M+1)(q+M+1)} &= \int_{S_2} \frac{dP_l(\nu_2)}{d\theta_2}\frac{1}{r_2}\frac{d}{dr_2}\left[r_2 h_q(k_s r_2)\frac{dP_q(\nu_2)}{d\theta_2}\right]dS_2, \quad n,q \neq 0;
\end{aligned} \tag{13}$$

$$\begin{aligned}
\mathbf{S}^{(1)}: S_{(l+1)(q+1)} &= \int_{S_1} P_l(\nu_1)\frac{d}{dr_1}[j_q(k_c r_1)P_q(\nu_1)]dS_1,\\
S_{(l+M+1)(q+1)} &= \int_{S_1} \frac{dP_l(\nu_1)}{d\theta_1}\frac{1}{r_1}\frac{d}{d\theta_1}[j_q(k_c r_1)P_q(\nu_1)]dS_1, \quad n\neq 0;\\
\mathbf{S}^{(2)}: S_{(l+1)(q+1)} &= \int_{S_2} P_l(\nu_2)\frac{d}{dr_2}[j_q(k_c r_2)P_q(\nu_2)]dS_2,\\
S_{(l+M+1)(q+1)} &= \int_{S_2} \frac{dP_l(\nu_2)}{d\theta_2}\frac{1}{r_2}\frac{d}{d\theta_2}[j_q(k_c r_2)P_q(\nu_2)]dS_2, \quad n\neq 0,
\end{aligned} \tag{14}$$

where $l,q = 0,1,\ldots,M$, unless otherwise stated. This system of equations is solved for the multipole coefficients of the scattered waves, B_n and C_n, of both spheres simultaneously. It is noted that the computation cost depends on the size of the square $\mathbf{K}$ matrix, which is $2\times(2M+1)$ for two spheres.

A. Primary radiation force

Calculation of the primary radiation force only depends on the incident wave and the scattered wave from each individual sphere. A series solution for the primary force has been proposed by Hasegawa and Yosioka for an ideal fluid by integrating the second-order tractions over the surface of a spherical particle [26]. That series solution is written as

$$\begin{aligned}
F_p &= 4\rho_0\pi|\Phi_0|^2\sin(2kL)Y_{st},\\
Y_{st} &= \sum_{n=0}^{\infty}(-1)^{n+1}[\mathrm{Im}(S_n) + 2(n+1)\\
&\quad\times\{\mathrm{Re}(S_{n+1})\mathrm{Im}(S_n) - [1+\mathrm{Re}(S_n)]\mathrm{Im}(S_{n+1})\}],
\end{aligned} \tag{15}$$

where Re(•) and Im(•) are the real and imaginary parts of a complex number, respectively; $S_n = B_n/A_n$ and B_n and A_n are the multipole coefficients of the scalar velocity potential of the incident and scattered waves, respectively. By using the far-field approach, it was shown later that the same series solution can be used for the case of a viscous fluid, except that the multipole coefficients B_n were obtained from the viscous boundary condition [19]. That series solution for the viscous case is hereafter referred to as the far-field series solution. For the jth sphere, the primary force, calculated from the far-field series solution, is expressed as

$$\begin{aligned}
F_p^{(j)} &= 4\rho_0\pi|\Phi_0|^2\sin(2kL_j)Y_{st}^{(j)},\\
Y_{st}^{(j)} &= \sum_{n=0}^{\infty}(-1)^{n+1}\big[\mathrm{Im}\big(S_n^{(j)}\big) + 2(n+1)\big\{\mathrm{Re}\big(S_{n+1}^{(j)}\big)\mathrm{Im}\big(S_n^{(j)}\big)\\
&\quad - \big[1+\mathrm{Re}\big(S_n^{(j)}\big)\big]\mathrm{Im}\big(S_{n+1}^{(j)}\big)\big\}\big],
\end{aligned} \tag{16}$$

where $S_n^{(j)} = B_n^{(j)}/A_n^{(j)}$ with $B_n^{(j)}$ obtained from Eq. (9) including the effect of the viscosity as well as the presence of the other sphere.

B. Total force

For calculating the total force acting on the spheres in a viscous fluid, we need to include the streaming of the fluid around the spheres driven by the acoustically induced body force. In this section, the numerical algorithm proposed in Ref. [20] is extended to the case of two spheres. As mentioned before, we assume that the fluid is stationary and its zero-order mean velocity is zero. In addition, it has been shown that the streaming flow induced by a plane standing wave is negligible [21,22]. Hence, the viscous drag due to the main flow and the incident streaming are neglected in this derivation. The total force, induced by the scattered waves, acting on the jth sphere is [21]

$$\begin{aligned}
\mathbf{F}^{(j)} = \int_{S_j}\Big\langle &\mu\big[\nabla\mathbf{v}_2^{(s)} + \big(\nabla\mathbf{v}_2^{(s)}\big)^T\big] + \Big(\xi - \frac{2}{3}\mu\Big)\\
&\times\nabla\cdot\mathbf{v}_2^{(s)}\mathbf{I} - p_2^{(s)}\mathbf{I}\Big\rangle\cdot\mathbf{n}dS - \int_{S_j}\rho_0\langle\mathbf{v_1}\otimes\mathbf{v_1}\rangle^{(s)}\cdot\mathbf{n}dS,
\end{aligned} \tag{17}$$

where n is the unit vector normal to the surface of the sphere and pointing outwards, $\mathbf{I}$ is the identity tensor, and $\mathbf{v}_2^{(s)}$ and $p_2^{(s)}$ are the second-order velocity and pressure induced by the scattered waves from all the spheres, respectively. The Reynolds stress in the second integral of Eq. (17) is expressed as

$$\rho_0\langle\mathbf{v}_1\otimes\mathbf{v}_1\rangle^{(s)} = \rho_0\big\langle\mathbf{v}_1\otimes\mathbf{v}_1 - \mathbf{v}_1^{(i)}\otimes\mathbf{v}_1^{(i)}\big\rangle, \tag{18}$$

where $\mathbf{v}_1^{(i)} = \nabla\phi_i$. The second-order variables are governed by the acoustic streaming equations, which are expressed as

$$\begin{aligned}
\rho_0\nabla\cdot\big\langle\mathbf{v}_2^{(s)}\big\rangle &= m_v,\\
-\nabla\big\langle p_2^{(s)}\big\rangle + \mu\nabla^2\big\langle\mathbf{v}_2^{(s)}\big\rangle + (\mu_B+\mu)\nabla\nabla\cdot\big\langle\mathbf{v}_2^{(s)}\big\rangle &= \mathbf{f}_v,
\end{aligned} \tag{19}$$

where

$$\begin{aligned}
m_v &= -\big(\nabla\cdot\langle\rho_1\mathbf{v}_1\rangle - \nabla\cdot\big\langle\rho_1^{(i)}\mathbf{v}_1^{(i)}\big\rangle\big),\\
\mathbf{f}_v &= \rho_0\big(\langle\mathbf{v}_1\cdot\nabla\mathbf{v}_1 + \mathbf{v}_1\nabla\cdot\mathbf{v}_1\rangle - \big\langle\mathbf{v}_1^{(i)}\cdot\nabla\mathbf{v}_1^{(i)} + \mathbf{v}_1^{(i)}\nabla\cdot\mathbf{v}_1^{(i)}\big\rangle\big),
\end{aligned} \tag{20}$$

and $\rho_1^{(i)} = i\rho_0 k^2\phi_1^{(i)}$. The second-order variables are split into the complementary and particular solutions as follows:

$$\begin{aligned}
\big\langle\mathbf{v}_2^{(s)}\big\rangle &= \big\langle\mathbf{v}_{2c}^{(s)}\big\rangle + \big\langle\mathbf{v}_{2p}^{(s)}\big\rangle,\\
\big\langle p_2^{(s)}\big\rangle &= \big\langle p_{2c}^{(s)}\big\rangle + \big\langle p_{2p}^{(s)}\big\rangle.
\end{aligned} \tag{21}$$

Since the scalar source term m_v can be neglected, the particular solutions of the second-order velocity and pressure can be calculated by the Stokeslet method [20,27]. For numerical implementation, a finite computational domain is required.

This domain is discretized by tetrahedral elements. Each element contains one Stokeslet source located at its centroid. For N number of elements, the particular solutions of the second-order variables are written as

$$\begin{aligned}\left\langle \mathbf{v}_{2p}^{(s)}\right\rangle\big|_{\hat{\mathbf{x}}_o} &= \sum_{n=1}^{N}\frac{\Omega_n}{8\pi\mu}\left(\frac{\mathbf{I}}{\hat{r}_n}+\frac{(\hat{\mathbf{x}}_n-\hat{\mathbf{x}}_o)\otimes(\hat{\mathbf{x}}_n-\hat{\mathbf{x}}_o)}{\hat{r}_n^3}\right)\mathbf{f}_v|_{\hat{\mathbf{x}}_n},\\ \nabla\left\langle p_{2p}^{(s)}\right\rangle\big|_{\hat{\mathbf{x}}_o} &= \sum_{n=1}^{N}\frac{\Omega_n}{4\pi\hat{r}_n^3}(\hat{\mathbf{x}}_n-\hat{\mathbf{x}}_o)\cdot\mathbf{f}_v|_{\hat{\mathbf{x}}_n},\end{aligned} \tag{22}$$

where $\hat{r}_n=|\hat{\mathbf{x}}_n-\hat{\mathbf{x}}_o|$, $\hat{\mathbf{x}}_n$ is the position vector of the centroid of the nth element, $\hat{\mathbf{x}}_o$ is the position vector of the observation point, at which the variables are calculated, $\mathbf{f}_v|_{\hat{\mathbf{x}}_n}$ is the vector source term evaluated at the element centroid, and Ω_n is the element volume.

The complementary solutions of the second-order velocity and pressure are related to the second-order velocity potentials as follows:

$$\begin{aligned}\left\langle \mathbf{v}_{2c}^{(s)}\right\rangle &= \nabla\overline{\phi}+\nabla\times\overline{\Psi},\\ \left\langle p_{2c}^{(s)}\right\rangle &= \mu\nabla^2\nabla\times\overline{\Psi}.\end{aligned} \tag{23}$$

For two spheres, those potentials are written as

$$\begin{aligned}\overline{\phi} &= \overline{\phi}^{(1)}+\overline{\phi}^{(2)},\\ \overline{\Psi} &= \overline{\Psi}^{(1)}+\overline{\Psi}^{(2)}.\end{aligned} \tag{24}$$

Since both second-order potentials are governed by harmonic equations derived from the streaming equation [20,22], they can be calculated using a multipole series expansion. For the jth sphere, the second-order potentials are written as

$$\begin{aligned}\overline{\phi}^{(j)} &= \sum_{n=0}^{\infty}\overline{B}_n\left(\frac{a_j}{r_j}\right)^{n+1}P_n(\nu_j),\\ \overline{\Psi}^{(j)} &= \mathbf{u}_{\varphi}^{(j)}\sum_{n=1}^{\infty}\frac{\overline{C}_n}{(4n-2)}\left(\frac{a_j}{r_j}\right)^{n-1}\frac{dP_n(\nu_j)}{d\theta_j},\end{aligned} \tag{25}$$

where a_j is the radius of the jth sphere, and $\overline{B}_n$ and $\overline{C}_n$ are the multipole coefficients of the second-order potentials. To obtain these multipole coefficients, the nonslip second-order viscous boundary conditions are imposed by the weighted residue technique as follows:

$$\begin{aligned}\int_{S^{(j)}}P_n(\nu_j)\left(\left\langle \mathbf{v}_2^{(s)}\right\rangle\cdot\mathbf{u}_r^{(j)}\right)dS=0,\\ \int_{S^{(j)}}\frac{dP_n(\nu_j)}{d\theta_j}\left(\left\langle \mathbf{v}_2^{(s)}\right\rangle\cdot\mathbf{u}_\theta^{(j)}\right)dS=0.\end{aligned} \tag{26}$$

The weights are again chosen due to orthogonality. For a pair of spheres, the set of equations obtained from the boundary conditions are written as

$$\begin{bmatrix}\overline{\mathbf{K}}^{(11)} & \overline{\mathbf{K}}^{(12)}\\ \overline{\mathbf{K}}^{(21)} & \overline{\mathbf{K}}^{(22)}\end{bmatrix}\begin{Bmatrix}\overline{\mathbf{B}}^{(1)}\\ \overline{\mathbf{C}}^{(1)}\\ \overline{\mathbf{B}}^{(2)}\\ \overline{\mathbf{C}}^{(2)}\end{Bmatrix}=-\begin{Bmatrix}\overline{\mathbf{S}}(1)\\ \overline{\mathbf{S}}^{(2)}\end{Bmatrix}. \tag{27}$$

It is noted that the truncation order of the multipole series expansion of the second-order potentials denoted by $\overline{M}$ is independent from that for the first-order potentials. The size of both the square submatrix $\overline{\mathbf{K}}$ and subvector $\overline{\mathbf{S}}$ is $2\overline{M}+1$. The elements of the $\overline{\mathbf{K}}$ and $\overline{\mathbf{S}}$ are expressed as follows:

$$\begin{aligned}\overline{\mathbf{K}}^{(11)}:\overline{K}_{(l+1)(q+1)} &= \int_{S_1}P_l(\nu_1)\frac{d}{dr_1}\left[\left(\frac{a_1}{r_1}\right)^{q+1}P_q(\nu_1)\right]dS_1,\\ \overline{K}_{(l+1)(q+\overline{M}+1)} &= \int_{S_1}\frac{P_l(\nu_1)}{r_1\sin\theta_1}\frac{d}{d\theta_1}\left[\frac{\sin\theta_1}{(4q-2)}\left(\frac{a_1}{r_1}\right)^{q-1}\frac{dP_q(\nu_1)}{d\theta_1}\right]dS_1,\quad q\neq 0,\\ \overline{K}_{(l+\overline{M}+1)(q+1)} &= \int_{S_1}\frac{dP_l(\nu_1)}{d\theta_1}\frac{1}{r_1}\frac{d}{d\theta_1}\left[\left(\frac{a_1}{r_1}\right)^{q+1}P_q(\nu_1)\right]dS_1,\quad n\neq 0,\\ \overline{K}_{(l+\overline{M}+1)(q+\overline{M}+1)} &= -\int_{S_1}\frac{dP_l(\nu_1)}{d\theta_1}\frac{1}{r_1}\frac{d}{dr_1}\left[\frac{r_1}{(4q-2)}\left(\frac{a_1}{r_1}\right)^{q-1}\frac{dP_q(\nu_1)}{d\theta_1}\right]dS_1,\quad n,q\neq 0;\end{aligned} \tag{28}$$

$$\begin{aligned}\overline{\mathbf{K}}^{(12)}:\overline{K}_{(l+1)(q+1)} &= \int_{S_1}P_l(\nu_1)\frac{d}{dr_1}\left[\left(\frac{a_2}{r_2}\right)^{q+1}P_q(\nu_2)\right]dS_1,\\ \overline{K}_{(l+1)(q+\overline{M}+1)} &= \int_{S_1}\frac{P_l(\nu_1)}{r_1\sin\theta_1}\frac{d}{d\theta_1}\left[\frac{\sin\theta_1}{(4q-2)}\left(\frac{a_2}{r_2}\right)^{q-1}\frac{dP_q(\nu_2)}{d\theta_2}\right]dS_1,\quad q\neq 0,\\ \overline{K}_{(l+\overline{M}+1)(q+1)} &= \int_{S_1}\frac{dP_l(\nu_1)}{d\theta_1}\frac{1}{r_1}\frac{d}{d\theta_1}\left[\left(\frac{a_2}{r_2}\right)^{q+1}P_q(\nu_2)\right]dS_1,\quad n\neq 0,\\ \overline{K}_{(l+\overline{M}+1)(q+\overline{M}+1)} &= -\int_{S_1}\frac{dP_l(\nu_1)}{d\theta_1}\frac{1}{r_1}\frac{d}{dr_1}\left[\frac{r_1}{(4q-2)}\left(\frac{a_2}{r_2}\right)^{q-1}\frac{dP_q(\nu_2)}{d\theta_2}\right]dS_1,\quad n,q\neq 0;\end{aligned} \tag{29}$$

$$\begin{aligned}\overline{\mathbf{K}}^{(21)}:\overline{K}_{(l+1)(q+1)} &= \int_{S_2}P_l(\nu_2)\frac{d}{dr_2}\left[\left(\frac{a_1}{r_1}\right)^{q+1}P_q(\nu_1)\right]dS_2,\\ \overline{K}_{(l+1)(q+\overline{M}+1)} &= \int_{S_2}\frac{P_l(\nu_2)}{r_2\sin\theta_2}\frac{d}{d\theta_2}\left[\frac{\sin\theta_2}{(4q-2)}\left(\frac{a_1}{r_1}\right)^{q-1}\frac{dP_q(\nu_1)}{d\theta_1}\right]dS_2,\quad q\neq 0,\end{aligned}$$

$$\overline{K}_{(l+\overline{M}+1)(q+1)} = \int_{S_2} \frac{dP_l(\nu_2)}{d\theta_2}\frac{1}{r_2}\frac{d}{d\theta_2}\left[\left(\frac{a_1}{r_1}\right)^{q+1} P_q(\nu_1)\right] dS_2, \quad n \neq 0,$$

$$\overline{K}_{(l+\overline{M}+1)(q+\overline{M}+1)} = -\int_{S_2} \frac{dP_l(\nu_2)}{d\theta_2}\frac{1}{r_2}\frac{d}{dr_2}\left[\frac{r_2}{(4q-2)}\left(\frac{a_1}{r_1}\right)^{q-1}\frac{dP_q(\nu_1)}{d\theta_1}\right] dS_2, \quad n,q \neq 0; \tag{30}$$

$$\overline{\mathbf{K}}^{(22)} : \overline{K}_{(l+1)(q+1)} = \int_{S_2} P_l(\nu_2)\frac{d}{dr_2}\left[\left(\frac{a_2}{r_2}\right)^{q+1} P_q(\nu_2)\right] dS_2,$$

$$\overline{K}_{(l+1)(q+\overline{M}+1)} = \int_{S_2} \frac{P_l(\nu_2)}{r_2 \sin\theta_2}\frac{d}{d\theta_2}\left[\frac{\sin\theta_2}{(4q-2)}\left(\frac{a_2}{r_2}\right)^{q-1}\frac{dP_q(\nu_2)}{d\theta_2}\right] dS_2, \quad q \neq 0,$$

$$\overline{K}_{(l+\overline{M}+1)(q+1)} = \int_{S_2} \frac{dP_l(\nu_2)}{d\theta_2}\frac{1}{r_2}\frac{d}{d\theta_2}\left[\left(\frac{a_2}{r_2}\right)^{q+1} P_q(\nu_2)\right] dS_2, \quad n \neq 0,$$

$$\overline{K}_{(l+\overline{M}+1)(q+\overline{M}+1)} = -\int_{S_2} \frac{dP_l(\nu_2)}{d\theta_2}\frac{1}{r_2}\frac{d}{dr_2}\left[\frac{r_2}{(4q-2)}\left(\frac{a_2}{r_2}\right)^{q-1}\frac{dP_q(\nu_2)}{d\theta_2}\right] dS_2, \quad n,q \neq 0; \tag{31}$$

$$\overline{\mathbf{S}}^{(1)} : \overline{S}_{(l+1)(1)} = \int_{S_1} P_l(\nu_1)\left(\left\langle \mathbf{v}_{2p}^{(s)}\right\rangle \cdot \mathbf{u}_r^{(1)}\right) dS_1,$$

$$\overline{S}_{(l+\overline{M}+1)(1)} = \int_{S_1} \frac{dP_l(\nu_1)}{d\theta_1}\left(\left\langle \mathbf{v}_{2p}^{(s)}\right\rangle \cdot \mathbf{u}_\theta^{(1)}\right) dS_1, \quad n \neq 0; \tag{32}$$

$$\overline{\mathbf{S}}^{(2)} : \overline{S}_{(l+1)(1)} = \int_{S_2} P_l(\nu_2)\left(\left\langle \mathbf{v}_{2p}^{(s)}\right\rangle \cdot \mathbf{u}_r^{(2)}\right) dS_2,$$

$$\overline{S}_{(l+\overline{M}+1)(1)} = \int_{S_2} \frac{dP_l(\nu_2)}{d\theta_2}\left(\left\langle \mathbf{v}_{2p}^{(s)}\right\rangle \cdot \mathbf{u}_\theta^{(2)}\right) dS_2, \quad n \neq 0, \tag{33}$$

where $l,q = 0,1,\ldots,\overline{M}$, unless otherwise stated. Similar to the set of equations derived for the first-order variables, the computation cost depends on the size of the $\overline{\mathbf{K}}$ matrix, which is $2 \times (2\overline{M}+1)$ for two spheres. After solving for the multipole coefficients $\overline{B}_n$ and $\overline{C}_n$, the complementary solutions of the second-order variables are obtained. The total force can be obtained from Eq. (17) for each individual sphere by combining the complementary solution from the multipole expansion and the particular solution from the Stokeslet method.

C. Special case of ideal fluid

For the special case of an ideal fluid, the acoustic velocity is obtained only from the gradient of the scalar potential ϕ. Since viscosity is absent, there is slippage of the fluid tangential to the particle surface; only a nonpenetrating boundary condition on the normal component of the velocity to the particle surface is enforced. There is no need to solve for the acoustic streaming, and the second-order stresses are the sum of the radiation pressure and the Reynolds stresses [24,28]. The current formulation can also be used for the case of an ideal fluid by ignoring the first-order vector potential Ψ and the acoustic streaming. The total force is calculated directly from the scattered wave potentials which were obtained by imposing the boundary conditions simultaneously [8,10]. It has been shown that the interparticle force can be derived separately from the force integral by accounting for cross-scattering terms [9,10].

To verify the current methodology, the results obtained for the case of ideal fluid are compared with those reported in Refs. [8,9]. A pair of 5-μm spheres ($ka = 0.03 \ll 1$) were considered with their centerline perpendicular to the wave direction as shown in Fig. 2(b). In Fig. 2(a), the vertical axis shows the normalized interaction force acting on sphere 1. It is noted that sphere 2 experiences a force with the same magnitude but in the opposite direction. The results are shown for various surface-to-surface distances. It can be seen that the current method gives accurate results for the interaction force, with the data overlapping with those obtained from Doinikov's method. This is expected since both methods are developed based on solving a fully coupled system of equations for multipole coefficients of the scattered waves. On the other hand, there is a gap between our results and those obtained from Silva and Bruus' formulation. This difference is due to the monopole-dipole approximation used for the scattered wave and the truncation in the rescattering approach used in their formulation.

III. RESULTS

In this section, we study the case of two identical rigid spheres located along the wave direction (axisymmetric configuration) and equally spaced from the pressure node, as shown in Fig. 3. A local spherical coordinate system is attached to each of them. The global coordinate system is located at the pressure node. The standing wave is in the z direction. The surface-to-surface distance between the two spheres is denoted by d. The size of the spheres is denoted by a. Due to the symmetrical configuration, the radiation forces acting on the spheres are equal and act in opposite directions. For numerical calculations, the water in STP condition (standard

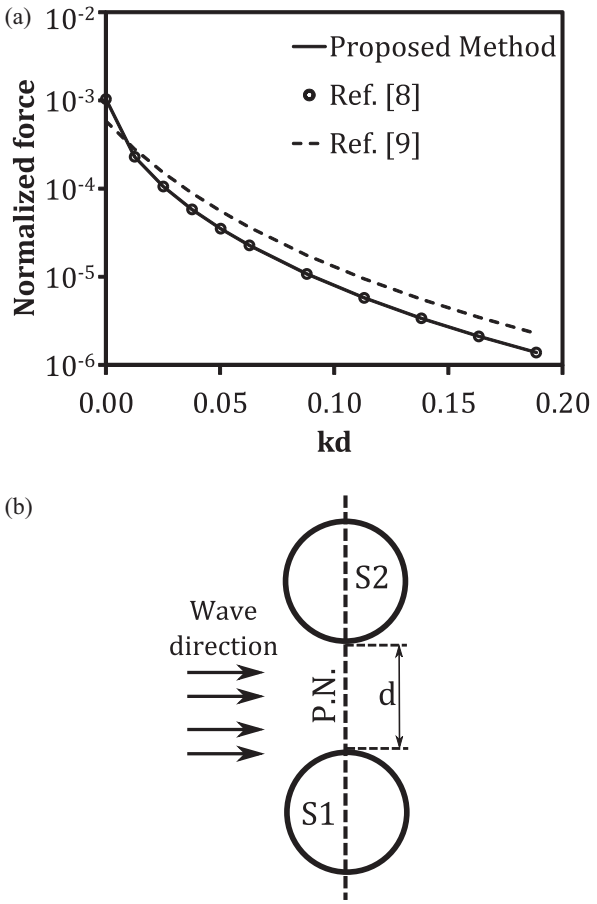

FIG. 2. (a) The normalized interparticle force between a pair of identical spheres of 5 μm size. (b) The spheres are positioned on the nodal plane (P.N.) of the incident wave which propagates in the z direction. The interaction force is normalized by $\frac{1}{2}\rho_0\Phi_0$, where Φ_0 is the amplitude of the incident velocity potential.

temperature and pressure) is considered as the host fluid. The frequency of the standing wave is 1.5 MHz and its wavelength is 1 mm. The pressure amplitude is set at 1 bar. For these parameters, the viscous penetration depth δ is 0.4 μm.

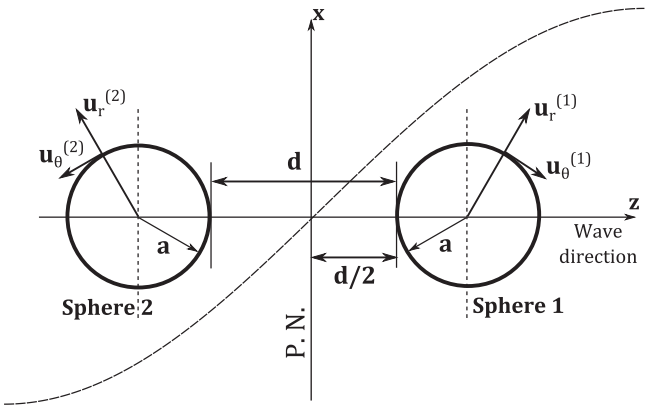

FIG. 3. Configuration of a pair of identical spheres equally spaced from the pressure node and positioned along the incident wave direction (the axisymmetric configuration).

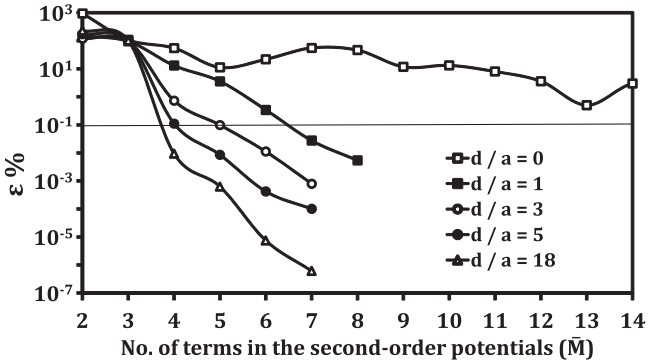

FIG. 4. Convergence test of the multipole series expansion of the second-order potentials for various surface-to-surface distances between a pair of 1-μm spheres.

A. Convergence test

Since the proposed numerical algorithm involves a series expansion, a convergence test is required for both the first- and second-order variables. The multipole series expansion of the first-order variables has been shown to be convergent and the number of terms included in the series calculation depends on the size of the sphere [20]. We hereby study the convergence of the second-order potentials for a pair of spheres. For this purpose, a truncation index is introduced as

$$\epsilon = \frac{\left|F(\overline{M}+1) - F(\overline{M})\right|}{\left|F(\overline{M}+1)\right|} \times 100\%, \tag{34}$$

where $F(\overline{M})$ is the total radiation force obtained from the first $\overline{M}$ terms included in the series expansion of the second-order potentials. In fact, ϵ shows the change of the total force by adding successive terms in the series calculation.

The truncation index ϵ calculated for various distances between a pair of 1-μm spheres is shown in Fig. 4. The desired accuracy of the series calculation is set to $\epsilon = 0.1\%$, shown as a horizontal line. For this set of results, the first eight terms were included in the first-order series computation ($M = 8$). When $d/a = 0$, the fluctuation of the truncation index implies that the results are not convergent. Therefore, the proposed numerical algorithm cannot be applied to the case of two spheres in contact with each other. For other values of d/a, convergence is achieved as the truncation index decreases monotonically, which means that adding more terms has a decreasing effect on the accuracy of the series calculation. Depending on the desired accuracy, the number of terms can be determined for different surface-to-surface distances. For example, for $d/a = 3$, five terms are required in the series calculation to achieve $\epsilon < 0.1\%$. By increasing the distance between the spheres, the number of terms required in the series becomes smaller due to the weaker interaction between them.

B. Primary radiation force

As described in Sec. II A, the primary radiation force has been calculated using the far-field series expansion for the two cases of a single sphere and a pair of spheres, as shown in Fig. 5(a). In Fig. 5(b), markers show the results for a pair of identical spheres of three different sizes for a wide range

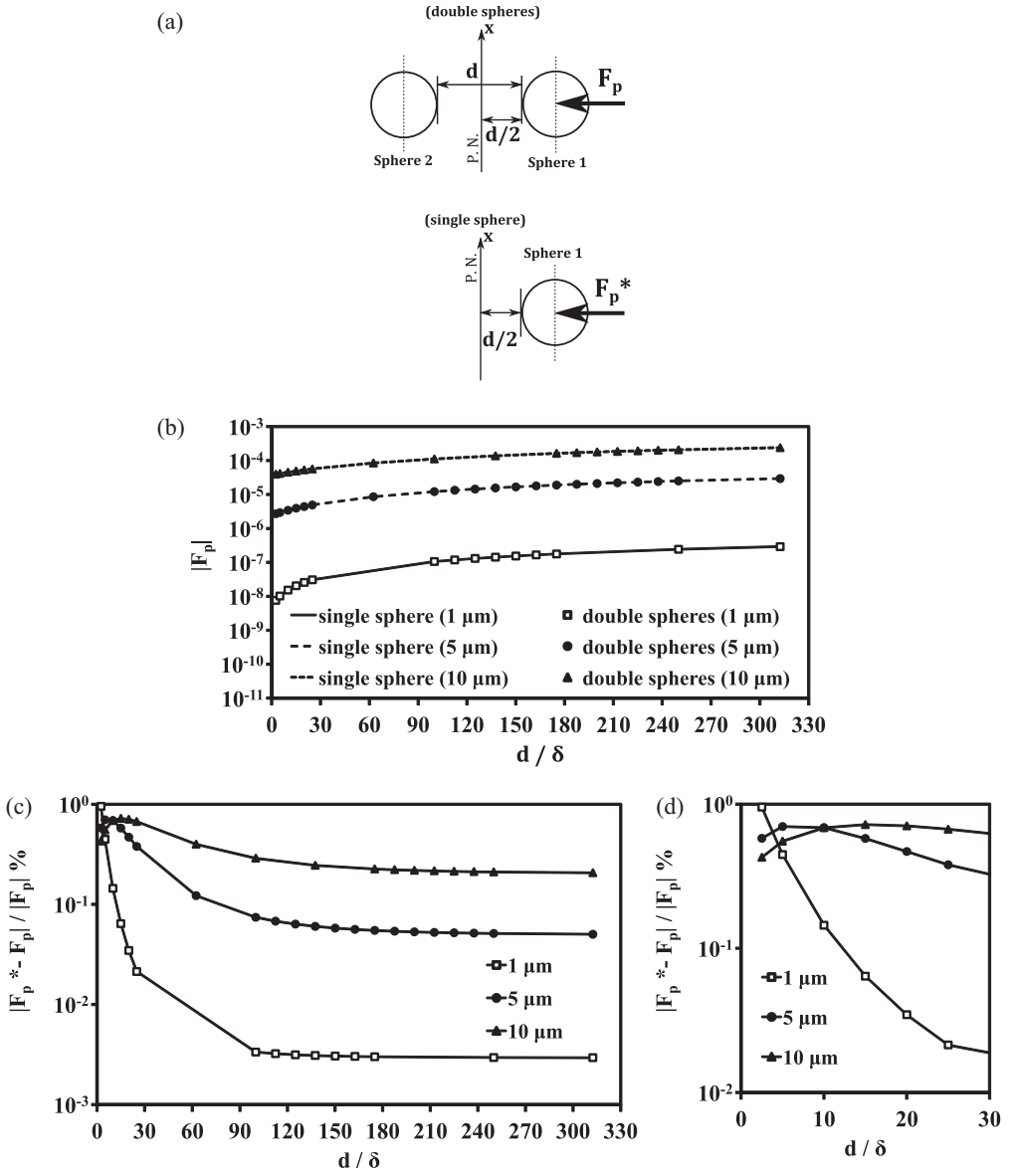

FIG. 5. In (a), two cases of single and double spheres in a standing wave are schematically shown. (b) shows the primary radiation force acting on sphere 1 for the two cases of one and two spheres. (c) shows the percentage difference between the two cases considering the case of two spheres as the reference. (d) shows the percentage difference for small values of d/δ.

of surface-to-surface distances d. Besides, the lines show the corresponding results for the case of a single sphere with the same distance from the pressure node. The differences between the primary forces calculated for the single- and double-sphere cases are very small and not visible for all sizes. It implies that the presence of the additional sphere in the fluid domain has insignificant effects on the primary radiation force acting on the target sphere. The relative difference between the two cases of one and two spheres has been calculated by considering the force for the double-sphere case (F_p) as the reference value. In Fig. 5(c), F_p^* is the force acting on the single sphere. It is shown that the presence of the second sphere changes the primary radiation force by less than 1%. As d increases, the influence of the second sphere decreases; thus, it can be neglected. For larger spheres, the change in the primary force is larger; however, it is still less than 1% for 10-μm spheres. It can be concluded that, for the case of two spheres, one can estimate the primary radiation force acting on each sphere by neglecting the presence of the other one.

C. Total radiation force

In Fig. 6(a), the magnitude of the total radiation force obtained from the multipole-Stokeslet method has been plotted in the logarithmic scale for three different sizes. It can be seen that the total radiation force increases as the spheres become larger. Discontinuities appear in the graphs where the total radiation force is zero, since it cannot be shown on the logarithmic scale. Each discontinuity hence represents a change in the direction of the total force, i.e., from repulsion to attraction. It is noted that the location of the zero total force is shifted away from the pressure node for larger spheres.

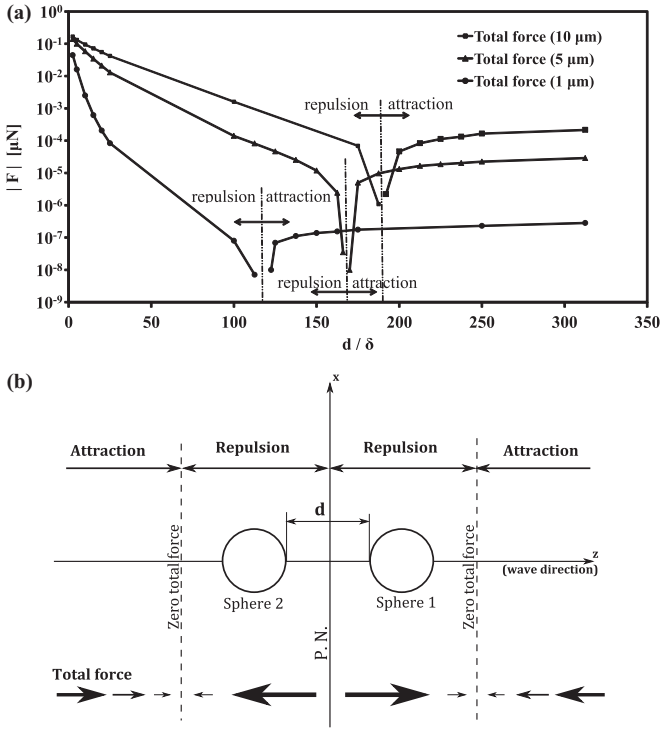

FIG. 6. (a) The magnitude of the total radiation force calculated by the proposed numerical scheme and (b) shown schematically for the case of two spheres.

Figure 6(b) shows the change in the total force schematically. If the centers of the two spheres fall in the region between the pressure node and the location of the zero total force, they tend to move away from each other (repulsion) under the total radiation force. If they are placed out of that region, they tend to move towards each other (attraction). In the vicinity of the pressure node $d/\delta \leqslant 1$, the repulsive total radiation forces are very large and have the same magnitude for all three sizes of the spheres.

In Fig. 7, the total radiation force has been calculated for a pair of spheres in both ideal [10] and viscous fluids. As mentioned before, the discontinuities in the graphs are where the total radiation force becomes zero and its direction is reversed (from repulsion to attraction). For small distances between the spheres, the repulsion forces calculated for the case of viscous and ideal fluid cases are of several orders of magnitude lower than the viscous cases. It is concluded that the effect of viscosity on the total radiation force is much greater when the spheres are located close to each other. For all three sizes of the spheres, the locations of the zero force for the viscous fluid are at further distances compared to the case of an ideal fluid. This is due to the stronger interaction between the two spheres in the viscous fluid. For large distances, the difference between the results obtained for the ideal and viscous cases tends to zero for the 5- and 10-μm spheres. For the 1-μm spheres placed far away from each other, the visible gap between the viscous and inviscid results implies that the viscosity and streaming have a larger effect on smaller spheres.

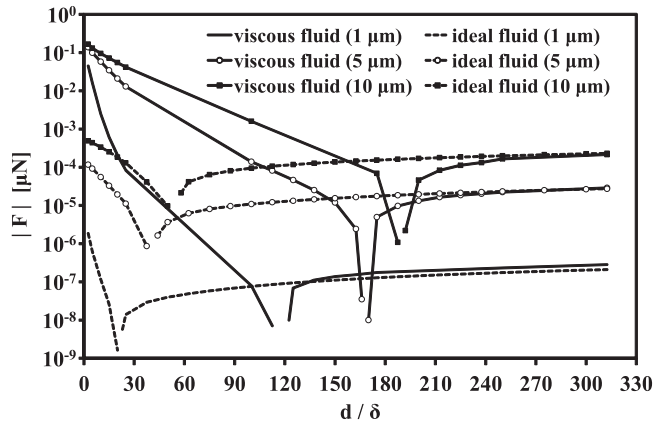

FIG. 7. Total radiation force calculated for both cases of ideal and viscous fluids.

D. Interparticle radiation force

Figure 8(a) shows the total and primary radiation forces over a wide range of d for three sizes of spheres. For a small value of d, the two spheres would be in the vicinity of the pressure node where the primary force is close to zero. However, the total force is observed to be several orders of magnitude larger than the primary force. It can be inferred that the interparticle force between the two spheres is dominant when the spheres are close to each other. For large distances between the two spheres, the total radiation force converges to the primary force for all three sizes of the

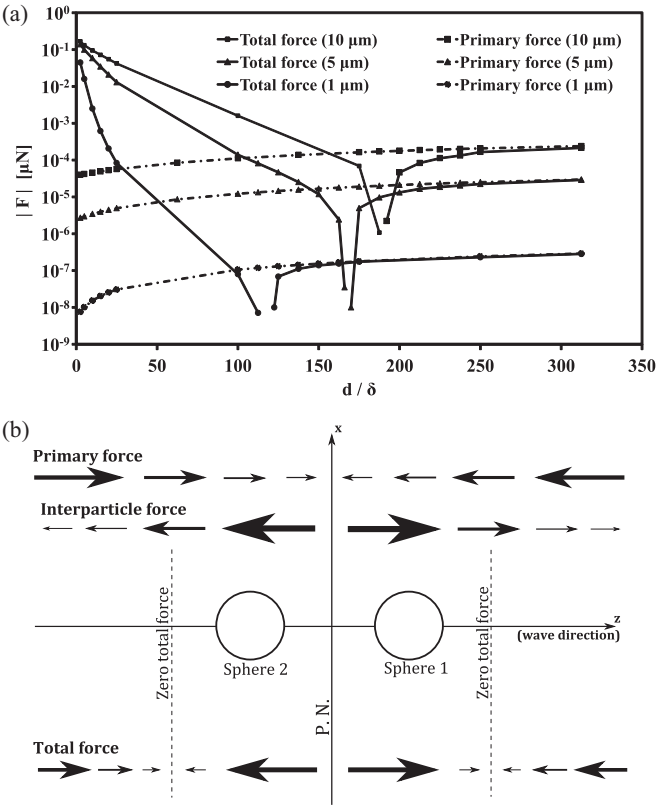

FIG. 8. (a) Comparing the total force against the primary force and (b) the schematic illustration of the total, primary, and interparticle forces.

spheres. This is expected since the interaction between the two spheres becomes considerably weak for large distances d. When the total radiation force becomes zero, the primary and the secondary (interparticle) forces balance each other. The interparticle radiation force is hereby estimated by subtracting the primary force from the total radiation force, i.e.,

$$F_s = F_{\text{tot}} - F_p. \tag{35}$$

It is noted that the estimated interparticle forces are repulsive in nature for the two spheres, regardless of the distance between them. The total, primary, and interparticle forces are schematically illustrated in Fig. 8(b).

In Fig. 9, the interaction between the two spheres has been approximated from Eq. (35). Two additional lines have been plotted to illustrate the effects of viscosity and streaming. The line with circle markers shows the interaction between the two spheres in an ideal fluid, calculated by the method proposed in Ref. [10]. It is assumed that the ideal fluid has the same density and compressibility as the viscous fluid. The line with square markers shows the results obtained for a pair of spheres in a viscous fluid without including the streaming effect. For this case, the second-order stresses are calculated from the time-averaged radiation pressure,

$$\langle \delta p \rangle = \frac{\rho_0}{2} \langle |\mathbf{v}_1|^2 \rangle - \frac{1}{2\rho_0 c_0^2} \langle p_1 \rangle, \tag{36}$$

which is valid for an ideal fluid. This means that the viscosity has been accounted for in the solution of the first-order variables only. The results shown by the solid line include the viscosity and streaming effects, as calculated by Eq. (35). These are the best estimations of the interaction between the two spheres in a viscous fluid.

For the 1-μm sphere, the clearly visible gap between the circle and square markers implies that the viscosity of the fluid increases considerably the interparticle forces between the two spheres for various d. However, the forces become much larger (about four orders of magnitude) by including the streaming effect, as shown by the solid line in Fig. 9(a). That gap becomes smaller for larger spheres, as shown in Figs. 9(b) and 9(c). It can be inferred that including the viscosity in the solution of the first-order variables has a more significant effect on the interaction between small spheres. It is also observed that the inclusion of the streaming effects increases the interparticle forces by two to three orders of magnitude even for the larger spheres. It implies that the interaction between the spheres is dominated by the acoustic streaming induced by their scattered waves, regardless of their size.

The interparticle forces acting on a pair of 5-μm spheres estimated for three different viscosity values are shown in Fig. 10. The forces are calculated for $0.2 < d/a < 10$, where the interaction between the spheres is strong. The interparticle force does not change drastically with the viscosity, as shown in Fig. 10(a). The force calculated for $\mu^* = 8.89 \times 10^{-4}$ [kg/(s mm)] (SI units) is considered as a reference value and denoted by $F(\mu^*)$. In Fig. 10(b), the results normalized by $F(\mu^*)$ have been plotted to better show the differences between the four sets of results. For $d/a > 0.4$, it is observed that the interparticle force becomes weaker by approximately 5%, 10%, and 15% for viscosity values of $\mu^*/2$, $\mu^*/5$, and $\mu^*/500$, respectively. For $d/a = 0.2$, the interaction between the spheres reduces further by 15%–20% for the four viscosity values. It is inferred that, for the viscous case, the increase in the interparticle force is due to the induced streaming around the spheres, even for a fluid with a very low viscosity.

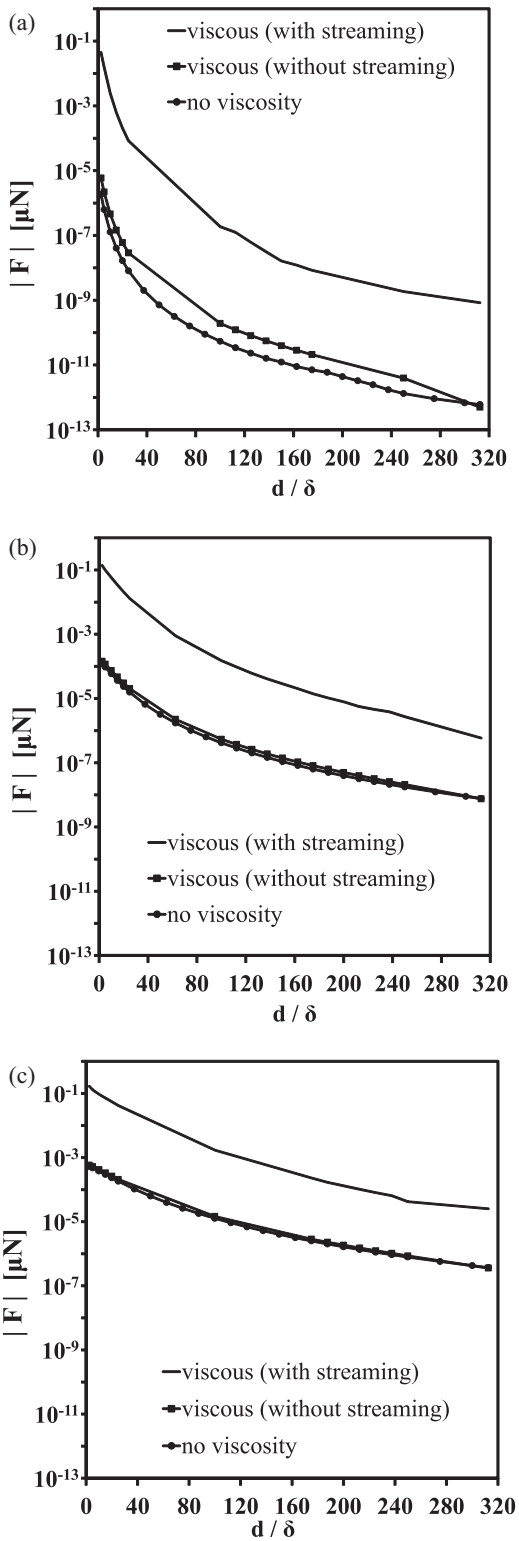

FIG. 9. Investigating the viscosity and acoustic streaming effects on the interparticle forces acting on a pair of identical spheres of (a) 1 μm, (b) 5 μm, and (c) 10 μm radius.

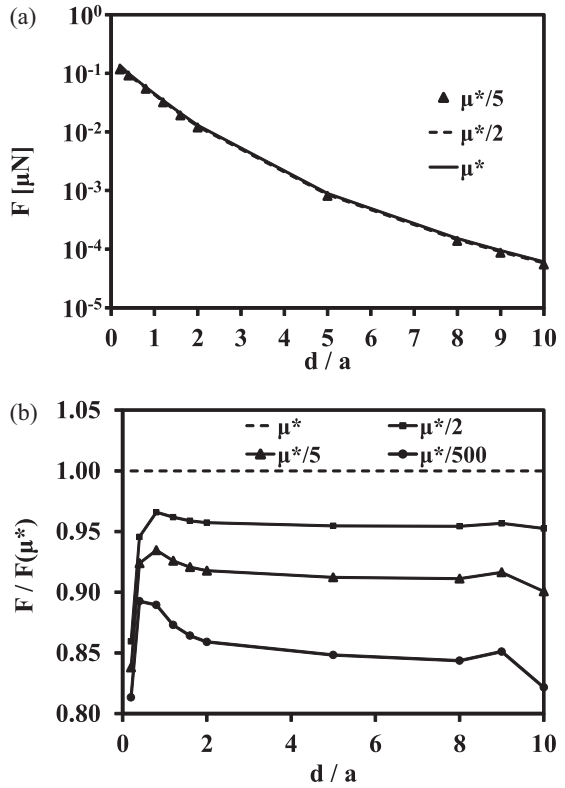

FIG. 10. (a) The interparticle forces for different viscosity values and (b) the relative difference between them.

IV. DISCUSSION

In this section, a simple order-of-magnitude analysis is performed on the second-order parameters and results. The acoustic velocity v_1 near the surface of each sphere reaches a maximum value due to the boundary effect. This maximum acoustic velocity for a 5-μm sphere in a 1.5 MHz standing wave with a pressure amplitude of 1 bar in water is of the order of 10^{-3} m/s. Thus, the order of magnitude of $\rho_0 v_1^2$ for the case of water would be 10^{-3} Pa. Considering the surface area of the 5-μm sphere, the force should be of the order of 10^{-12} N. This simple order-of-magnitude analysis gives a good estimate for the force that is consistent with the results shown in Fig. 9 for a pair of 5-μm spheres when they far apart from each other.

The above analysis is not valid when the spheres are close to each other due to the additional hydrodynamic interaction generated from the acoustic streaming around them. The results presented so far illustrate that the hydrodynamic interaction is significantly larger than the acoustical interaction obtained from the first-order variables. This means that, in laboratory-on-a-chip and acoustofluidics applications with viscous fluids, acoustic streaming has a significant effect on the acoustic interaction among particles clustered near each other.

V. CONCLUSION

A multipole-Stokeslet algorithm has been proposed to estimate the interparticle force from the solutions of the total and primary radiation forces. The numerical scheme is not restricted by the number of spheres and their sizes; however, the solution is not convergent for the spheres in contact with each other. To investigate the viscosity and streaming effects, the interparticle forces were calculated for a pair of identical spheres located along the wave direction (axisymmetric configuration) in a viscous fluid. It was found that acoustic streaming contributes significantly to the interaction between the spheres, as the interaction force increases by three orders of magnitude compared to that from the inviscid theory [10].

[1] L. A. Crum, Bjerknes forces on bubbles in a stationary sound field, J. Acoust. Soc. Am. **57**, 1363 (1975).
[2] A. A. Doinikov, Dissipative effects on Bjerknes forces between two bubbles, J. Acoust. Soc. Am. **102**, 747 (1997).
[3] A. A. Doinikov and S. T. Zavtrak, On the mutual interaction of two gas bubbles in a sound field, Phys. Fluids **7**, 1923 (1995).
[4] A. A. Doinikov and S. T. Zavtrak, Interaction force between a bubble and a solid particle in a sound field, Ultrasonics **34**, 807 (1996).
[5] A. A. Doinikov and S. T. Zavtrak, Radiation forces between two bubbles in a compressible liquid, J. Acoust. Soc. Am. **102**, 1424 (1997).
[6] A. A. Doinikov and S. T. Zavtrak, On the "bubble grapes" induced by a sound field, J. Acoust. Soc. Am. **99**, 3849 (1996).
[7] N. A. Pelekasis, A. Gaki, A. A. Doinikov, and J. A. Tsamopoulos, Secondary Bjerknes forces between two bubbles and the phenomenon of acoustic streamers, J. Fluid Mech. **500**, 313 (2004).
[8] A. A. Doinikov, Acoustic radiation interparticle forces in a compressible fluid, J. Fluid Mech. **444**, 1 (2001).
[9] G. T. Silva and H. Bruus, Acoustic interaction forces between small particles in an ideal fluid, Phys. Rev. E **90**, 063007 (2014).
[10] S. Sepehrirahnama, K.-M. Lim, and F. S. Chau, Numerical study of interparticle radiation force acting on rigid spheres in a standing wave, J. Acoust. Soc. Am. **137**, 2614 (2015).
[11] A. P. Zhuk, Hydrodynamic interaction of two spherical particles due to sound waves propagating perpendicularly to the center line, Int. Appl. Mech. **21**, 307 (1985).
[12] X. Zheng and R. E. Apfel, Acoustic interaction forces between two fluid spheres in an acoustic field, J. Acoust. Soc. Am. **97**, 2218 (1995).
[13] G. C. Gaunaurd and H. Huang, Sound scattering by a spherical object near a hard flat bottom, IEEE Trans. Ultrason. Ferroelectr. Freq. Control **43**, 690 (1996).
[14] H. Huang and G. C. Gaunaurd, Scattering of a plane acoustic wave by a spherical elastic shell near a free surface, Int. J. Solids Struct. **34**, 591 (1997).
[15] G. C. Gaunaurd, Acoustic scattering by an air-bubble near the sea surface, IEEE J. Oceanic Eng. **20**, 285 (1995).

[16] H. Huang and G. C. Gaunaurd, Acoustic scattering of a plane wave by two spherical elastic shells above the coincidence frequency, J. Acoust. Soc. Am. **101**, 2659 (1997).
[17] G. C. Gaunaurd, H. Huang, and H. C. Strifors, Acoustic scattering by a pair of spheres, J. Acoust. Soc. Am. **98**, 495 (1995).
[18] M. Settnes and H. Bruus, Forces acting on a small particle in an acoustical field in a viscous fluid, Phys. Rev. E **85**, 016327 (2012).
[19] S. Annamalai, S. Balachandar, and M. K. Parmar, Mean force on a finite-sized spherical particle due to an acoustic field in a viscous compressible medium, Phys. Rev. E **89**, 053008 (2014).
[20] S. Sepehrirahnama, K.-M. Lim, and F. S. Chau, Numerical analysis of the acoustic radiation force and acoustic streaming around a sphere in an acoustic standing wave, Phys. Procedia **70**, 80 (2015).
[21] A. A. Doinikov, Acoustic radiation pressure on a compressible sphere in a viscous fluid, J. Fluid Mech. **267**, 1 (1994).
[22] A. A. Doinikov, Acoustic radiation pressure on a rigid sphere in a viscous fluid, Proc. R. Soc. London, Ser. A **447**, 447 (1994).
[23] N. A. Gumerov and R. Duraiswami, *Fast Multipole Methods for the Helmholtz Equation in Three Dimensions* (Elsevier, Amsterdam, 2005).
[24] L. V. King, On the acoustic radiation pressure on spheres, Proc. R. Soc. London, Ser. A **147**, 212 (1934).
[25] H. Bruus, Acoustofluidics 7: The acoustic radiation force on small particles, Lab Chip **12**, 1014 (2012).
[26] T. Hasegawa and K. Yosioka, Acoustic radiation force on a solid elastic sphere, J. Acoust. Soc. Am. **46**, 1139 (1969).
[27] J. Wang and J. Dual, Time-averaged acoustic force and torque exerted on an arbitrarily shaped rigid particle in a viscous fluid using boundary element method, in *International Congress on Ultrasonics: Gdańsk 2011*, AIP Conf. Proc. No. 1433 (AIP, Melville, NY, 2012), pp. 791–794.
[28] K. Yosioka and Y. Kawasima, Acoustic radiation pressure on a compressible sphere, Acustica **5**, 167 (1955).